Equivalent Wire-Grids for the Electromagnetic Modeling of Conducting Surfaces

Tony Golden
ansof@antennasimulator.com
Research & Development, Golden Engineering Ltd.

Abstract- A novel approach to model metallic surfaces by means of wire-grids is presented. We establish a theoretical basis for partitioning the surface into thin flat strips that then can be replaced by wires having an equivalent radius, which can be calculated from well-known formulas for planar dipoles. Numerical examples show that the proposed model is not sensitive to the choice of the wire radius and that the so-called equal area rule for wire-grid modeling is not supported by our approach.

Index Terms- Wire equivalent radius, Method of Moments, metallic surfaces, equivalent wire-grids, wire-grid model, equal area rule.

I. INTRODUCTION

Here an equivalent wire-grid model for the calculation of scattering and radiation by solid conducting surfaces is presented. The modeling of metallic surfaces by means of wire-grids is still attractive due to its simplicity and because algorithms written specifically for wire structures can be easily extended for the modeling of surfaces. Wire-grids have been investigated in the past in the frame of the Method of Moments (MoM) and some guidelines for choosing the wire length and radius have been deducted from the observation of numerical results and validated by measurements [1], [2], [3], [4]. In particular, the so-called "equal area rule" (EAR) or "same surface area" has become widely used in Numerical Electromagnetics Code (NEC) wire-grid models [5], [6], [7], [8]. The EAR states that the wire segment area must equal the surface patch area being modeled by the wire-grid, so the wire radius can be obtained from this area. For the case of square patches, the EAR radius is then $1/(2\pi)$ of the square side. This is a rule of thumb that has been applied over the years with relative success; however it does not have a theoretical justification and a way to demonstrate it from the Electromagnetics first principles cannot be easily visualized. Since numerical results have been reported to be very sensitive to the wire radius, the choice of the optimum radius is still considered to be an art [3], [6], [7], [8].

This article will establish a theoretical basis for the choice of the wire-grid radii and will show that the EAR is not a universal rule and that is actually associated with the particular implementation of the MoM in NEC. From an Electric Field Integral Equation (EFIE) an equivalent wire-grid model for general solid conducting surfaces will be obtained. A surface will be first modeled by a grid of flat strips whose widths are chosen to cover the whole surface. Then, it will be shown that the strips can be replaced by cylindrical wire segments with an equivalent radius. Moreover, the equivalent radius of a flat strip in the grid equals 0.22 of the strip width, which is a well-known theoretical result obtained for an isolated conducting strip in free space [9]. Therefore, an equivalent radius supported by theory different from the EAR radius will be obtained.

This paper is organized as follows. In section II, the EFIE and the MoM in the frequency domain used to calculate the current distribution on surfaces and wire-grids are described. Section III reviews the concept of equivalent radius, which is then used to deduce the equivalent radius for strip grids in Section IV. The EAR is described in Section V to show the differences with the theoretical equivalent radius obtained in Section IV. These results are then validated by numerical examples of canonical closed surfaces in Section VI, where the total electric field must vanish inside the surfaces when an external plane wave impinges on the structure. In the case of a small sphere compared to the wavelength, the MoM calculations satisfactorily reproduce the closed-form equations of the external scattered field just on the sphere surface, which shows that the proposed model can also be applied to the prediction of near fields.

II. METHOD OF MOMENTS FOR SURFACES AND WIRES

The MoM is a numerical technique extensively applied to solve integral equations in Electromagnetics [1]. In the case of perfectly conducting surfaces, an EFIE can be obtained from the boundary condition of zero total tangential electric field on the surfaces. There is a variety of formulations for the EFIE with pros and contras depending of the ulterior application of the MoM [10]. We will consider the following formulation:

$$\hat{\boldsymbol{n}} \times \frac{j}{\omega\varepsilon} \iint_S \left[k^2 \boldsymbol{J}(\boldsymbol{r}') \, G(\boldsymbol{r}, \boldsymbol{r}') + \nabla' \cdot \boldsymbol{J}(\boldsymbol{r}') \, \nabla G(\boldsymbol{r}, \boldsymbol{r}') \right] dS' = \hat{\boldsymbol{n}} \times \boldsymbol{E}_i \tag{1}$$

where $\boldsymbol{E}_i$ is the incident electric field at the observation point $\boldsymbol{r}$ on the surface S, $\hat{\boldsymbol{n}}$ is the unit vector normal to S at $\boldsymbol{r}$, $\boldsymbol{J}$ is the electric current density at the source point $\boldsymbol{r}'$, $k = 2\pi/\lambda$ is the wave number, λ is the wavelength, $\omega = 2\pi f$ is the angular frequency, f is the frequency in Hertz, ε is the dielectric constant of free space, and G is the free space Green's function given by

$$G(\boldsymbol{r}, \boldsymbol{r}') = \frac{e^{-jk\,|\boldsymbol{r}-\boldsymbol{r}'|}}{4\pi\,|\boldsymbol{r}-\boldsymbol{r}'|} \tag{2}$$

Note that the left-hand side of (1) is the tangential component of the scattered electric field at $\boldsymbol{r}$ and that G has a singularity at $\boldsymbol{r} = \boldsymbol{r}'$. If we consider a general curved surface that is described by a parametric function, such as $\boldsymbol{r} = \boldsymbol{r}(u, v)$, $u_0 \le u \le u_U$, $v_0 \le v \le v_V$, the vector current density can be expressed in terms of its scalar components J_u and J_v,

$$\boldsymbol{J}(u, v) = J_u(u, v)\,\hat{\boldsymbol{u}} + J_v(u, v)\,\hat{\boldsymbol{v}} \tag{3}$$

where $\hat{\boldsymbol{u}}$ and $\hat{\boldsymbol{v}}$ are tangent unit vectors to the surface, so $\hat{\boldsymbol{n}} = \hat{\boldsymbol{u}} \times \hat{\boldsymbol{v}}$, and can be obtained from the first partial derivatives of $\boldsymbol{r}(u, v)$ [10].

We can also define the impedance operator Z that acts on a scalar function $J = J(u, v)$ as follows:

$$Z_{uv}\,J = \frac{j}{\omega\varepsilon} \iint_S \left[\, k^2\, J(u', v')\; \hat{\boldsymbol{u}} \cdot \hat{\boldsymbol{v}}'\; G(u, v, u', v') + \nabla' \cdot J(u', v') \hat{\boldsymbol{v}}'\; \hat{\boldsymbol{u}} \cdot \nabla G(u, v, u', v') \,\right] du'\, dv' \tag{4}$$

Then, (1) can be written as a set of two integral equations,

$$\begin{aligned} Z_{uu}\,J_u + Z_{uv}\,J_v &= \boldsymbol{E}_i \cdot \hat{\boldsymbol{u}} \\ Z_{vu}\,J_u + Z_{vv}\,J_v &= \boldsymbol{E}_i \cdot \hat{\boldsymbol{v}} \end{aligned} \tag{5}$$

We can see that if the surface parameterization is chosen so that $\hat{\boldsymbol{u}}$ and $\hat{\boldsymbol{v}}$ are mutually orthogonal for all u and v, then $\hat{\boldsymbol{u}} \cdot \hat{\boldsymbol{v}} = 0$ and the first term in (4) vanishes for Z_{uv} and Z_{vu}. This is an important result since we will obtain a reduced number of calculations by choosing an orthogonal description of the surface.
The impedance operator in (5) is linear, so the MoM can be applied to transform the EFIE into a system of linear equations of finite order. After expanding the current density components into a set $\{F_n\}$ of N basis functions and projecting the resulting sum on a set $\{T_m\}$ of N testing functions, we obtain

$$\begin{aligned} \sum_n \left[\, \langle T_m,\, Z_{uu} F_n \rangle J_{u,n} + \langle T_m,\, Z_{uv} F_n \rangle J_{v,n} \,\right] &= \langle T_m, E_u \rangle \\ \sum_n \left[\, \langle T_m,\, Z_{vu} T_n \rangle J_{u,n} + \langle T_m,\, Z_{vv} F_n \rangle J_{v,n} \,\right] &= \langle T_m, E_v \rangle \end{aligned} \tag{6}$$

which is a set of linear equations of order $2N \times 2N$ with unknown coefficients $\left[J_{u,n},\, J_{v,n}\right]$ and where $E_u = \boldsymbol{E}_i \cdot \hat{\boldsymbol{u}}$ and $E_v = \boldsymbol{E}_i \cdot \hat{\boldsymbol{v}}$.
This is a quite general formulation where we have not yet made any approximation on the integrals involved and nothing is said about the choice of the basis and testing functions. For calculations to be manageable in practice, it is usual to choose functions that are defined on small regions of S compared to the wavelength and that are canceled in the rest of the surface [11]. To do this, we can partition the surface into quasi-rectangular regions by dividing the domain of $\boldsymbol{r} = \boldsymbol{r}(u, v)$ into segments along u and v: $u_0 < u_1 < \cdots < u_U$ and $v_0 < v_1 < \cdots < v_V$. We will obtain in this way a surface partition as depicted in Fig. 1. We then realize that the surface can be seen as if it were made up of two sets of strips, namely, one set $S(u, v_n)$ along the u coordinate and another set $S(u_n, v)$ along the v coordinate. Thus, Z_{uu} describes the self and mutual interactions of strips within the set $S(u, v_n)$, Z_{vv} describes the self and mutual interactions within the set $S(u_n, v)$, while Z_{uv} and Z_{vu} describe the mutual interactions between both sets of surface strips.

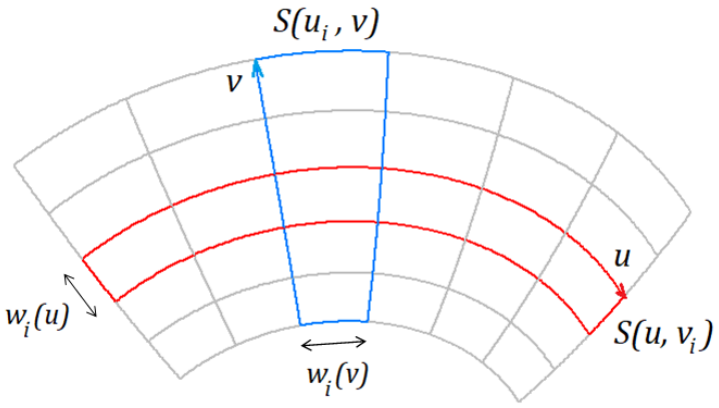

Fig. 1: Partition of a surface S into small regions compared to the wavelength, so $w_i(u), w_i(v) \ll \lambda$. The surface can be viewed as made up of two sets of thin strips along two independent directions, u and v.

If we focus on Z_{uu} interactions and isolate a single strip $S(u, v_i)$, we will obtain (4) with $\hat{\boldsymbol{v}}' = \hat{\boldsymbol{u}}'$ and $J = J_u(u, v)$. Furthermore, if the strip width is small enough compared to the wavelength, we can assume that its current density is uniform with respect to v, so (4) is reduced to a line integral along the u coordinate and (5) reduces to

$$\frac{j}{\omega\varepsilon}\int_{S(u,v_i)}\left[\, k^2\, I(u')\, K(u,u')\, \hat{\boldsymbol{u}}\cdot\hat{\boldsymbol{u}}' + \frac{dI(u')}{du'}\,\frac{\partial K(u,u')}{\partial u}\right] du' = E_u \tag{7}$$

where $K(u,u')$ is the kernel of this integral equation that can be obtained by integrating the Green's function in (2) with respect to v and v' across the strip cross section. Equation (7) is actually the EFIE for a thin wire to be solved for the current distribution $I(u)$. We can also see that the cross section shape of the thin wire only affects the kernel K locally, in a neighborhood of $u = u'$. When u and u' are on different strips, (7) represents the mutual interaction between the strips. Note also that (7) does not assume a straight wire, but a general curved wire with tangent unit vector $\hat{\boldsymbol{u}}$. Thus, we will not approximate the strips by means of straight segments, but we will use the curvilinear EFIE in (7) for the application of the MoM [12], [13]. We will call this MoM implementation as the Curvilinear Method of Moments (CMoM) to distinguish it from the traditional straight wire implementation used in NEC. Regarding the width, w, of the strip $S(u, v_i)$, it will be a function of the position, u, along the strip and can be calculated as follows:

$$w_i(u) = \int_{v_i}^{v_{i+1}} \left|\frac{\partial \boldsymbol{r}(u,v)}{\partial v}\right| dv \;\cong\; |\boldsymbol{r}(u, v_{i+1}) - \boldsymbol{r}(u, v_i)| \tag{8}$$

An identical analysis can be applied by isolating a strip $S(u_i, v)$ along the v coordinate, consequently we realize that the other terms in (5) and (6) are mutual interaction terms between crossing strips on the surface. Thus, we have come to the conclusion that a conducting surface can be viewed as composed of strips which extend along and across the surface in two independent directions. Besides, each strip can be viewed as a thin wire with a "flat" cross section when the strip widths are small enough compared to the wavelength. Having the widths in (8), the strips cover the whole surface without leaving holes between them. To fill the MoM matrix in (6) then we have to calculate self and mutual interactions between the segments into which the strips have been divided.

III. THE CONCEPT OF EQUIVALENT RADIUS

The electromagnetic behavior of thin wires having a circular cross section has been treated and approached theoretically several times in the literature [14], [15], [16]. It is well known that this solution can be extended to thin wires having a non-circular cross section by calculating an equivalent radius [17]. So, the actual cross section can be replaced by an equivalent circular cross section which produces the same near field and input impedance as the actual wire. In the case of a conducting flat strip of width w, by using a spectral domain approach to study planar dipoles, Rhodes [9] has established that the equivalent radius, a_e, is given by

$$a_e = e^{-3/2}\, w \;\cong\; 0.22\, w \tag{9}$$

As a matter of fact, we have already found in (7) that the kernel of the EFIE for a thin strip is affected by the shape of the strip cross section only locally, when the observation point is near to the source point. So, looking for an equivalent radius is just a matter of equalizing the kernels between the actual cross section and a circular one, and this is what is at the heart of the procedure to arrive at (9). Based on a quasi-static approximation to the magnetic vector potential in the wire cross section, Hallén [18] has found a

somewhat different equivalent radius for the flat strip, namely, $a_e = 0.25\,w$. However, this difference is not significant as we will see later, since the electromagnetic response of the equivalent wire-grids is found to be not very sensitive to the choice of the radius.
We should emphasize that (9) is a result supported theoretically and therefore it does not depend on the numerical method being used to calculate the current distribution on a wire. Furthermore, a well-implemented numerical method should reproduce this theoretical result.

IV. EQUIVALENT WIRE-GRID MODEL OF A SURFACE

Having defined the surface strips and revisited the concept of equivalent radius, we are now ready to build an accurate wire-grid model for conducting surfaces. As we have seen, to calculate the impedance matrix elements in (6) we have to compute self and mutual interactions between the two sets of strips the surface is made of. So, we can identify three kinds of interactions that will be described in the following.

A. Interaction of a strip with itself

Under the assumption of a strip width smaller enough than the wavelength, we can use the CMoM developed in Section II where only a line integral along the strip length must be computed for obtaining the impedance matrix elements of a single strip. Under this condition, we can also apply the equivalent radius in (9). Thus, this is just the same well-known MoM procedure that applies to thin cylindrical wires. However, the radius will possible vary along the wire since the strip width *w* will generally vary along its length, as (8) shows. For a smooth enough variation of the wire radius this is not a problem in a well-implemented MoM, where the basis functions are chosen to assure the continuity of the current distribution. We can also point out that the so-called thin-wire approximation could be used for the kernel in (7) if the wire radius is small enough compared to the wavelength and to the segment length, where the source point is considered to be on the wire axis and the observation point on the wire surface [1]. Thus, the thin-wire kernel approximation for the strips will be given by

$$K(u,v,u',v') = \frac{e^{-jkR}}{4\pi R}$$
$$R = \sqrt{|\boldsymbol{r}(u,v) - \boldsymbol{r}(u',v')|^2 + (0.22\,w(u,v))^2} \tag{10}$$

B. Mutual interactions between quasi-parallel strips

Strips that are "quasi-parallel" to each other are those that belong to the same set. For instance, let us take the strips in the set $S(u,v_n)$. The mutual interaction between the strips $S(u,v_i)$ and $S(u,v_{i+p})$, with $p \neq 0$, can be calculated in the same way we calculate the interaction between two quasi-parallel thin wires, where we can use the equivalent radius in (9) and the thin-wire approximation (10) in the integral equation's kernel. Thus, the source point at $S(u,v_i)$ can be considered to be on the wire axis and the observation point at $S(u,v_{i+p})$ on its surface, and vice versa. The width of the strips in (8) prevents them from overlapping each other and also covers the whole surface along u, as Fig. 2 shows. Care must be taken when computing the interaction between neighboring strips, $S(u,v_i)$ and $S(u,v_{i+1})$, since the integrands will increase strongly when the source and observation points are close to each other, so an iterative quadrature algorithm should be used to compute the integrals in this case [10]. An identical analysis can be applied to the strips $S(u_n,v)$.

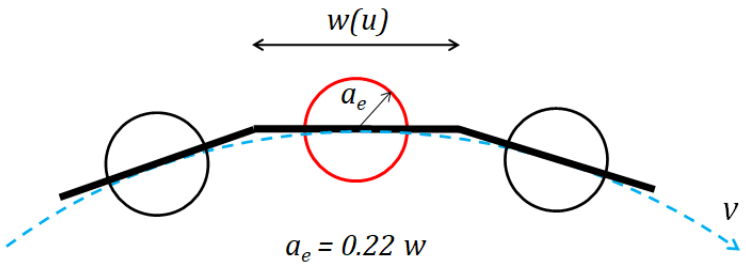

Fig. 2: Quasi-parallel strips along the *u* direction (*u* leaves the page). A cut of the surface at *u* = constant is shown, where the cross section of the strips having width *w* can be seen. Each strip can be replaced by a wire of an equivalent radius $a_e = 0.22w$.

C. Mutual interactions between crossing strips

For two strips that belong to different sets, the same treatment as for quasi-parallel strips can be applied. So, we will use an equivalent radius and a thin-wire kernel to compute the impedance matrix elements when the observation point at $S(u, v_i)$ is far enough from the source point at $S(u_p, v)$. At the point where the strips intersect, we must compute the mutual impedance matrix elements carefully. Additional conditions must be added to ensure compliance with Kirchhoff's law at the junction between the equivalent wires, but this depends on the particular implementation of the MoM [1], [10]. For instance, if we use triangular basis functions along the wires, Kirchhoff's law is automatically satisfied by adding just one bent basis function at the junction, as Fig. 3 shows. In the case of NEC, sinusoidal basis functions are used and conditions on the derivative of the current distribution are then applied at the junction between wires [5]. An additional simplification of the calculations can be obtained if an orthogonal description of the surface is adopted, since the first term in (4) goes to zero as we have pointed out previously.

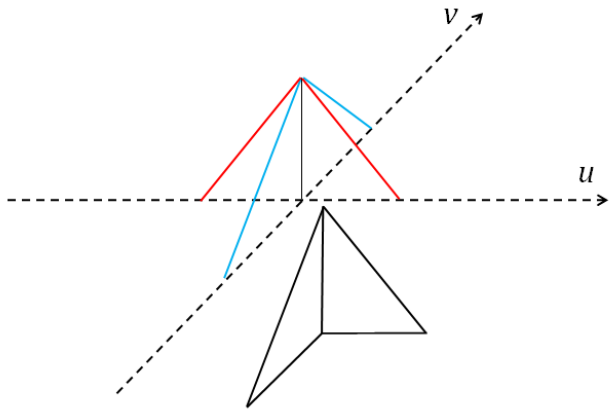

Fig. 3: Junction between crossing strips. Only the axes of the strips along the independent directions u and v are shown. Kirchhoff's law must be assured at the connection point, which is accomplished by adding one bent basis function at the junction when triangular basis functions are used in the MoM.

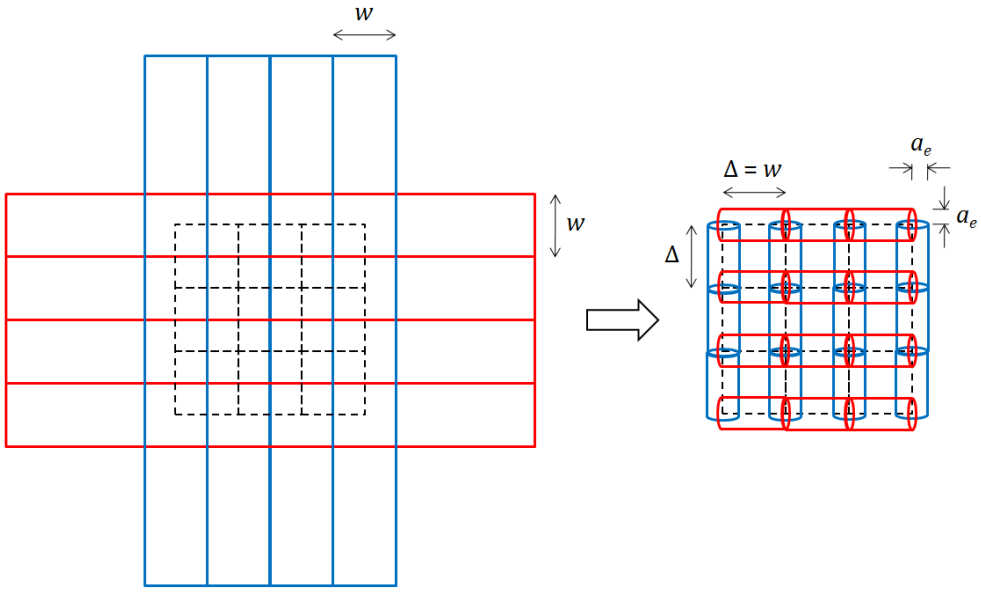

Fig. 4: Modeling of a flat surface using an orthogonal equivalent wire-grid. The surface is first partitioned into uniform strips of width w and then the strips are replaced by wires of radius $a_e = 0.22w$. The wire segment length will be equal to the strip width, $\Delta = w$.

As a summary, the wire-grid model we have built consists of dividing the surface into thin strips along two independent directions, the strip widths being smaller enough than the wavelength. We then apply the MoM replacing the strips by thin wires with an equivalent radius, which allows us to approximate double integrals using line integrals. The equivalent radius at each point on the surface equals 0.22 of the strip width. We have to notice that the current distributions $I(u)$ and $I(v)$ obtained by solving the system of linear equations in (6) will be expressed in Amperes, so the components of the current density can be obtained by dividing the currents into the strip width at each point. From the current density distribution the near and far fields can be calculated. Since the equivalent radius is just an artifact to approximate double integrals using equivalent line integrals, in fact there are no holes in the surface model, so the wire-grid model proposed here should reproduce faithfully the near fields even on the surface, where the electric field is perpendicular to the surface at each point. The numerical example of a conducting sphere in Section VI will validate this expected result for the radial component of the electric field.

Fig. 4 shows the case of a flat surface partitioned into strips of uniform width, *w*, of an orthogonal representation. It is interesting to note that, if the surface were modeled by a mesh of wire segments in the traditional way, the segment length, Δ (or the side of the square "holes"), will be equal to *w*, so the equivalent wire-grid radius will be given by

$$a_e = 0.22\,\Delta \tag{11}$$

V. THE EQUAL AREA RULE

The EAR is a numerical guideline documented for the NEC implementation of the MoM [6], [7], [8]. Let us consider a wire-grid model of a conducting surface that consists of square patches, each patch being delimited by four wire segments of radius a and length Δ. Then, the EAR states that the wire segment area, $2\pi a\Delta$, must equal the square patch area, Δ^2. Therefore, the EAR radius may be calculated as

$$a = \frac{\Delta}{2\pi} \cong 0.16\,\Delta \tag{12}$$

It is not clear how this rule could be extended to wire-grids of arbitrary shape; however, it has been proposed to consider the average of the patch areas on each side of a wire segment [8]. Following the calculations throughout the preceding sections, it does not seem possible to find a theoretical justification for this rule. Furthermore, the proposed equivalent wire-grid model should refute the EAR, since the difference between equations (11) and (12) is evident. As a matter of fact, the numerical examples in Section VI will be found to satisfy the theoretical equivalent radius in (11) rather than the EAR in (12).

VI. NUMERICAL EXAMPLES

The CMoM for wire structures has been implemented from the general curvilinear EFIE in (7), where we will choose triangular basis and pulse testing functions to expand the current distribution and the electric field, respectively, as it is depicted in Figs. 5(a) and 5(b).

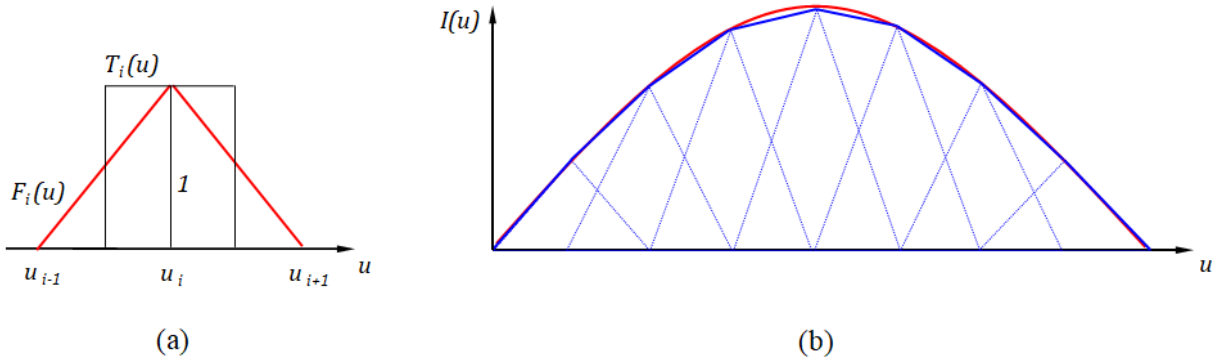

Fig. 5: (a) Triangular basis and pulse testing functions used in the CMoM to expand the current distribution and weight the electric field along a thin strip. (b) Example of a current distribution along a thin strip obtained from the CMoM and represented by the triangular basis functions.

The inner product in (6) is a line integral of the field along the wires weighted by the pulse testing functions. In addition, we will allow two parallel wires to be very close to each other by calculating carefully the integrals involved when the observation point is very

close to the source point. Therefore, this CMoM satisfies the conditions described in Section IV to model conducting surfaces by means of equivalent wire-grids. The thin-wire kernel in (10) will be used to compute mutual interaction terms, while the full kernel will be used to calculate self-terms. We must remark again that the wire-grid model we have developed does not leave holes in the surface because the strips have widths that completely cover the surface.
In Ref. [19] it has been shown that the EAR minimizes the total electric field inside the closed surface of a cube. This is a good indicator of the model validity since the total field inside a perfect Faraday cage must be equal to zero. In addition to the cube case, below we will show the numerical results for a closed conducting cylinder and a sphere.

A. Cube

The closed surface of a metallic cube will be modeled by an orthogonal equivalent wire-grid. The frequency and cube dimensions are the same as those used in Ref. [19], so f = 300 MHz (λ = 1 m) and the cube side is 40 cm long. The surface will be partitioned into uniform strips of width w = 4 cm ($w = 0.04\lambda$), which corresponds to the mesh wire spacing Δ used in Ref. [19]. Then, the equivalent radius given by (11) is a_e = 8.8 mm, while the EAR radius given by (12) is 6.4 mm. A linearly polarized plane wave with an E-field of 1 V/m is illuminating the cube and the vertical and oblique polarizations will be analyzed.
Fig. 6(a) shows the cube where the strips covering the surface have been replaced by lines representing the equivalent wire axes. The total electric field calculated using the CMoM at the cube center as a function of the wire radius, a, is plotted in Fig. 6(b), where we would expect that the optimal wire radius is the one that minimizes the total E-field. The NEC results extracted from Ref. [19] are also shown for comparison. We can see that each minimum is obtained for the radius predicted by the corresponding model. So the EAR radius should always be used in NEC, while the equivalent radius a_e in the CMoM. However, the NEC response is very sensitive to the wire radius compared to the CMoM, which has a much smoother variation. In fact, the result is practically the same for radii between 7 and 11 mm in the CMoM, so we could choose any a/w between 0.18 and 0.28 to model the cube surface.

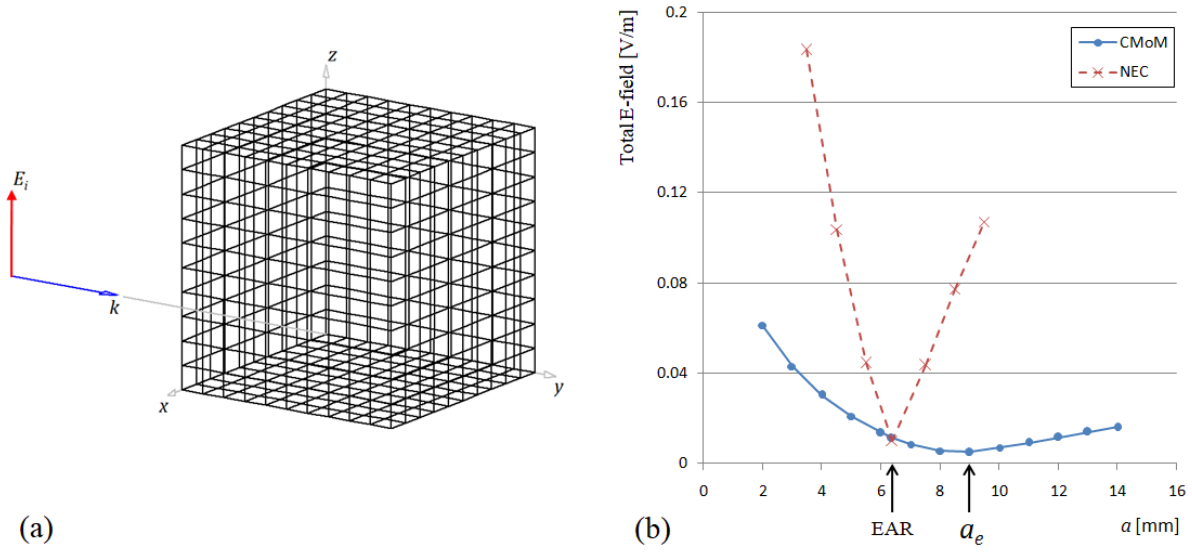

Fig. 6: (a) Plane wave with vertical polarization illuminating a metallic cube modeled by an equivalent CMoM wire-grid. (b) Total E-field at the cube center as a function of the wire radius. The EAR radius and the strips equivalent radius are indicated.

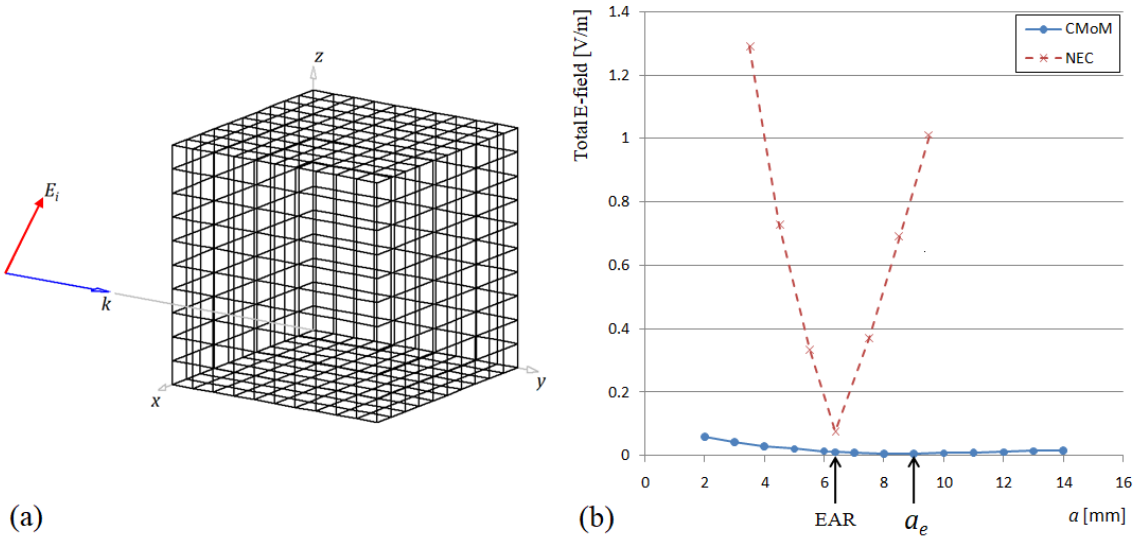

Fig. 7: (a) Plane wave with oblique polarization illuminating a metallic cube modeled by an equivalent CMoM wire-grid. (b) Total E-field at the cube center as a function of the wire radius. The EAR radius and the strips equivalent radius are indicated.

Fig. 7(a) shows the same metallic cube as in Fig. 6(a) but with an incident E-field having oblique polarization (45° inclination with respect to the vertical *z* axis). The CMoM total E-field at the cube center is plotted in Fig. 7(b) as a function of the wire radius and the NEC results from Ref. [19] are also shown. We can see again a sharp behavior of the NEC field where the values go beyond zero quickly for radii different than the EAR, even exceeding 1 V/m for radii less than 5 mm or greater than 10 mm. On the contrary, a smooth behavior and field values near zero are obtained in the CMoM calculation for a wide range of radii.

The authors in Ref. [19] also analyze the case of a triangular mesh approximation to the surface. They expected a better performance of the triangular mesh compared to the square mesh but they found, on the contrary, that the radius predicted by the EAR is far from the radius that minimizes the field inside the cube. The triangular mesh also fails to reproduce the experimental results. We can explain this behavior if we realize that a triangular mesh would cause the linear system in (6) to be overdetermined because we would have three linearly dependent directions on the surface instead of two independent directions. In other words, the current density along the diagonal direction in a triangular mesh can be obtained from a linear combination of its linearly independent components (mutually orthogonal components for the cube), so there's no point in adding a diagonal component in this case.

B. Cylinder

A closed cylinder 40 cm in diameter and 40 cm in height has been modeled by a CMoM equivalent wire-grid as Fig. 8(a) shows, so the cylinder size is similar to the size of the cube analyzed previously. The frequency is also f = 300 MHz. The cylinder surface has been partitioned into strips of a uniform width, w = 4 cm, while the cylinder caps have been modeled by using strips of varying widths following equation (8). Thus, the cylinder caps are modeled by an equivalent wire-grid of varying radii. A plane wave with an E-field of 1 V/m illuminates the cylinder and two linear polarizations will be considered, one parallel to the cylinder axis and the other perpendicular to it. Fig. 8(b) shows the total E-field at the cylinder center as a function of the uniform wire radius used in the cylinder surface, so the wire radii in the caps remain unchanged. In the case of vertical polarization (solid line), the field changes faster compared to the cube case, but the field values are anyway very low for radii between 7 and 11 mm as for the cube. The minimum field is obtained for a = 8 mm (a/w = 0.2), in close agreement with the equivalent radius of 8.8 mm (a/w = 0.22). Regarding horizontal polarization, Fig. 8(b) (dashed line) shows an even smother behavior, where the field becomes practically independent of the wire radius for radii between 10 and 14 mm (a/w between 0.25 and 0.35). Thus, the equivalent radius given by (9) is an optimal choice also for the closed cylinder.

From the point of view of traditional wire-grid modeling, it is always intended that the mesh be uniform over the entire surface, so the grid used in the cylinder caps would be considered to be too dense at the center of each disc. Nevertheless, we are modeling under the CMoM scheme, where we have no limitations to use dense grids as long as the guidelines described in Section IV are respected. Therefore, as long as the widths of the strips are small enough with respect to the wavelength, our effort should be concentrated on carefully calculating the matrix elements of the linear system in (6). Also, in many cases it is easier to choose an orthogonal wire-grid than to cover the surface with a uniform grid. This happens in the following example of a conducting sphere.

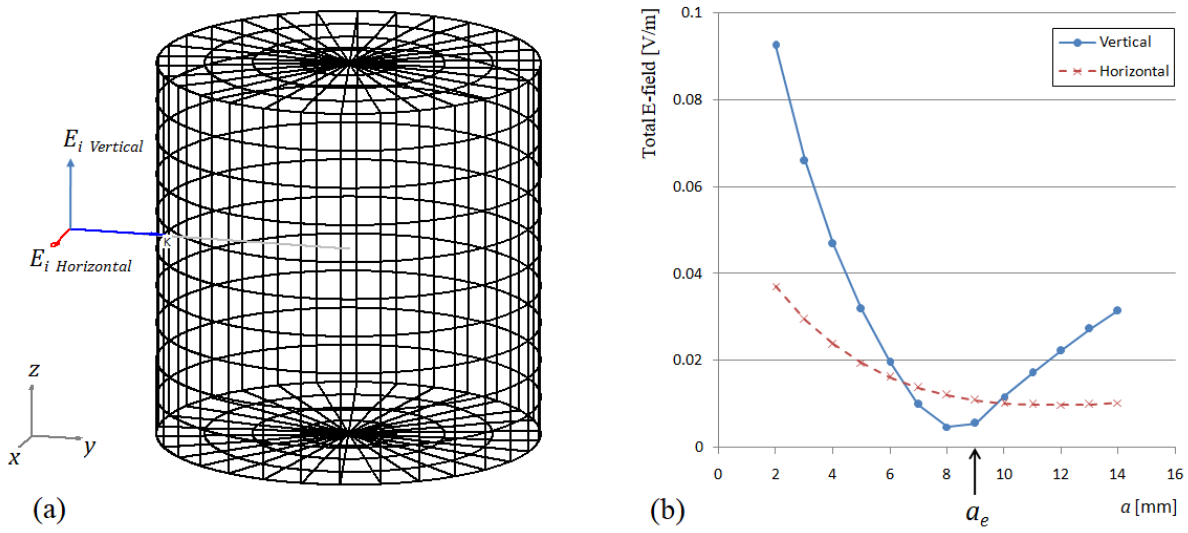

Fig. 8: (a) Plane wave illuminating a metallic closed cylinder modeled by an equivalent CMoM wire-grid. (b) Total E-field at the cube center as a function of the wire radius for two cases: vertical (solid line) and horizontal (dashed line) polarizations. The strips equivalent radius is indicated.

C. Sphere

A conducting sphere is an interesting canonical surface since simple closed form expressions are known for the scattered field when the sphere diameter is much smaller than the wavelength [20]. Fig. 9(a) shows the CMoM wire-grid model of a sphere 40 cm in diameter, so its size is similar to the cube and cylinder analyzed before. A linearly polarized wave with an E-field of 1 V/m illuminates the sphere at a frequency of 300 MHz. The width of each strip varies along its length and has been calculated using equation (8), which reduces to the simple calculation of an arc length on the spherical surface. The widest strip is 4 cm wide. Since the equivalent wires will also have varying radii, the total E-field at the sphere center has been calculated as a function of the ratio a/w and is shown in Fig. 9(b). The behavior of the field is similar to that obtained for the cylinder in vertical polarization, the variation is not so smooth but the field values are still very low, especially for a/w between 0.2 and 0.25. The minimum field is obtained for a/w = 0.22, so the agreement with equation (9) is remarkable, as in the cube case.

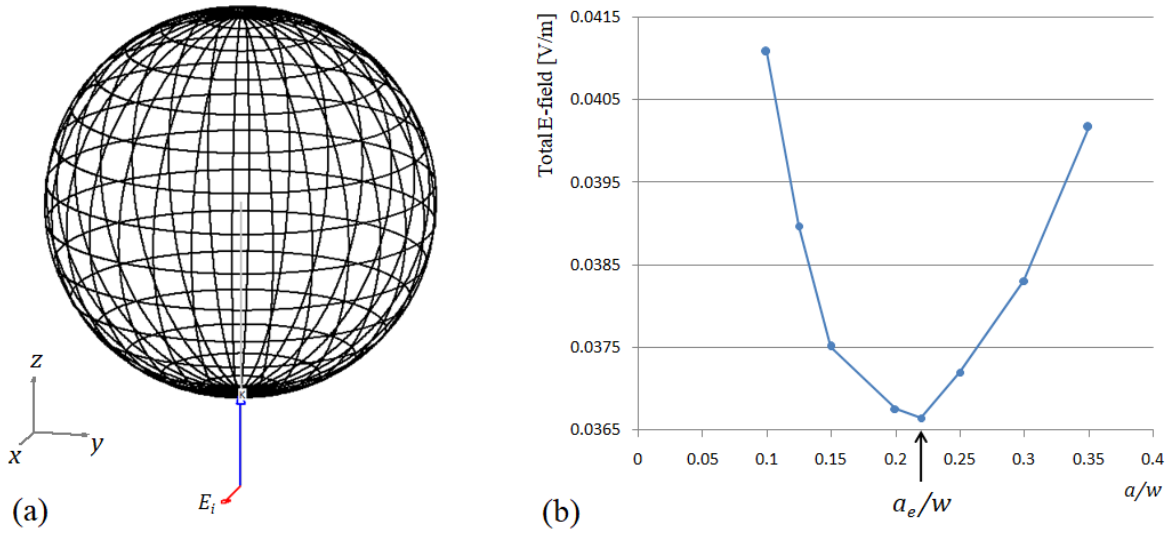

Fig. 9: (a) Linearly polarized plane wave illuminating a metallic sphere modeled by an equivalent CMoM wire-grid. (b) Total E-field at the sphere center as a function of the wire radius to strip width ratio. The strips equivalent radius is indicated.

If we now decrease the frequency to f = 3 MHz (λ = 100 m), the diameter of the sphere measured in wavelengths will be decreased 100 times, so a closed form expression can be obtained for the scattered field under this condition. With respect to the coordinate system shown in Fig. 9(a), if the 1 V/m incident field is polarized along the x-axis, the radial component of the scattered E-field will be given by [20]

$$E_r = 2 \sin\theta \cos\varphi \tag{13}$$

where (θ, φ) are the standard spherical coordinates, $0 \leq \theta \leq 180°$ and $0 \leq \varphi \leq 360°$. Fig. 10(a) shows the amplitude of the radial component (perpendicular to the surface) of the scattered E-field calculated by means of the CMoM just on the sphere surface. We can see that a maximum of 2 V/m is obtained at (θ, φ) = (90°, 0°) and (90°, 180°), and a null field is obtained at φ = 90° and φ = 270° for all θ, in close agreement with equation (13). Fig. 10(b) shows the same plot as in Fig. 10(a) with the zx plane in the plane of the page (the y-axis leaves the page towards the reader).

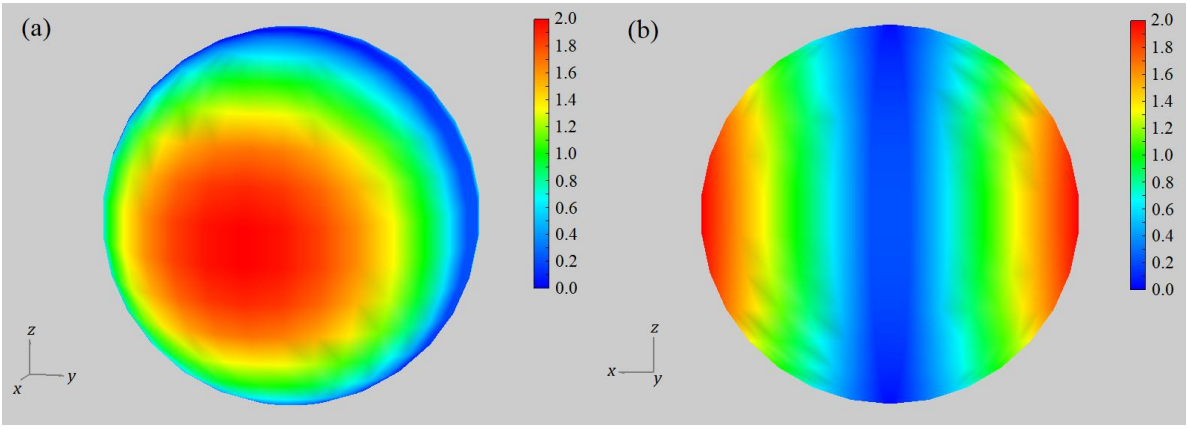

Fig. 10: (a) Color map of the radial component of the scattered E-field calculated via the CMoM just on the surface of the sphere when a 1 V/m incident field polarized along the x-axis illuminates the sphere at 3 MHz. (b) Same as (a) looking at the sphere from the y-axis. The color scale is in V/m. Sphere diameter is 40 cm.

Two slices of the field map in Fig.10 are plotted in Fig. 11. Fig. 11(a) shows the scattered E-field at φ = 0 as a function of θ, while Fig. 11(b) shows the field at θ = 90° as a function of φ, where the solid line corresponds to equation (13) and the dots are the values calculated via the CMoM. The agreement between the CMoM and theory is remarkable taking into account that these are near field calculations just on the equivalent wire-grid model of the sphere surface.

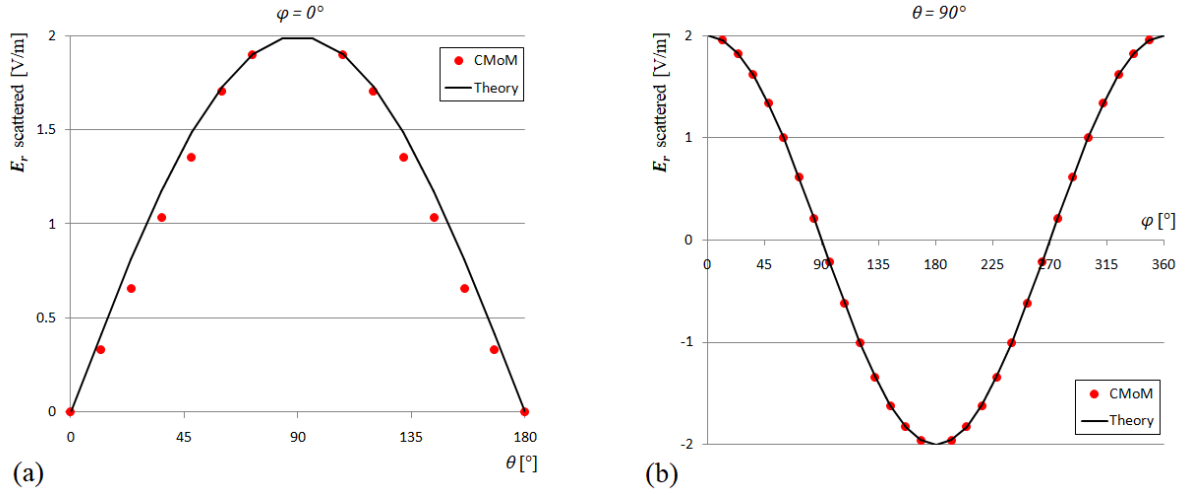

Fig. 11: Radial component of the scattered E-field just on the sphere surface, (a) at φ = 0 as a function of θ, (b) at θ = 90° as a function of φ. Sphere diameter is 40 cm, f = 3 MHz, 1 V/m incident field polarized along x-axis.

VII. CONCLUSIONS

We have established a theoretical frame for the modeling of conducting surfaces using equivalent wire-grids where the wire radius is well defined. The Method of Moments has been applied to an Electric Field Integral Equation for a general curved surface described by a parametric function. The parametric description is a function of two independent directions along and across the surface. This allows us to define strips that cover the whole surface after partitioning the parametric domain. If the widths of the strips are smaller enough than the wavelength, then each strip can be replaced by a thin wire having an equivalent radius. The wire-grid obtained in this way is equivalent to the original conducting surface since they both have the same electromagnetic response. It has been found that the equivalent wire radius can be calculated using the same well-known expression as for an isolated thin flat strip. The numerical results obtained for the closed surfaces of a cube, a cylinder and a sphere validate the choice of the equivalent radius proposed here. The electromagnetic response of these surfaces shows a behavior that is not very sensitive to the wire radius in a wide range of values, as opposed to what is obtained in wire-grid modeling using the Numerical Electromagnetics Code. It is also found that the Equal Area Rule is not predicted by theory nor reproduced in the results we have obtained. Due to the generality of our analysis, it is expected that this equivalent wire-grid modeling frame can be extended to surfaces that are not in free space, as in the case of planar antennas on dielectric substrates.

REFERENCES

[1] R.F. Harrington, *Field Computation by Moment Methods*, MacMillan, New York, 1968.

[2] J.H. Richmond, "A Wire-Grid Model for Scattering by Conducting Bodies," IEEE Trans. Antennas Propagat., Vol. AP-14, No. 6, pp. 782-786, Nov. 1966.

[3] K.S.H. Lee, L. Marin and J.P. Castillo, "Limitations of Wire-Grid Modeling of a Closed Surface," IEEE Trans. on Electromagn. Compatibility, Vol. EMC-18, No. 3, pp. 123-129, Aug. 1976.

[4] J.T. Mayhan, "Characteristic Modes and Wire Grid Modeling," IEEE Trans. Antennas Propagat., Vol. 38, No. 4, pp. 457-469, Apr. 1990.

[5] G. Burke and A. Poggio, "Numerical Electromagnetics Code - Method of Moments," Livermore CA: Lawrence Livermore National Lab., Report No. UCID-18834, 1981.

[6] A.C. Ludwig, "Wire Grid Modeling of Surfaces," IEEE Trans. Antennas Propagat., Vol. 35, No. 9, pp. 1045-1048, Sept. 1987.

[7] R.J. Paknys, "The Near Field of a Wire Grid Model," IEEE Trans. Antennas Propagat., Vol. 39, No. 7, pp. 994-999, July 1991.

[8] C.W. Trueman and S.J. Kubina, "Fields of Complex Surfaces using Wire Grid Modeling," IEEE Trans. on Magnetics, Vol. 27, No. 5, pp. 4262-4267, Sept. 1991.

[9] D.R. Rhodes, "On a Fundamental Principle in the Theory of Planar Antennas," Proc. IEEE, Vol. 52, No. 9, pp. 1013–1021, Sept. 1964.

[10] B.D. Popović and B.M. Kolundžija, *Analysis of Metallic Antennas and Scatterers*, The Institution of Electrical Engineers, London, UK, 1994.

[11] J.M. Song and W.C. Chew, "Moment Method Solutions Using Parametric Geometry," J. of Electromagnetic Waves and Appl., Vol. 9, No. 1/2, pp. 71-83, Jan-Feb. 1995.

[12] N.J. Champagne II, J.T. Williams and D.R. Wilton, "The Use of Curved Segments for Numerically Modeling Thin Wire Antennas and Scatterers," IEEE Trans. Antennas Propagat., Vol. 40, No. 6, pp. 682-689, June 1992.

[13] S.D. Rogers and C.M. Butler, "An Efficient Curved-Wire Integral Equation Solution Technique," IEEE Trans. Antennas Propagat., Vol. 49, No. 1, pp. 70-79, Jan. 2001.

[14] J.D. Kraus, *Antennas*, Mc. Graw Hill, N. Y., 1950, 1988, 2002.

[15] C.A. Balanis, *Antenna Theory Analysis and Design*, John Wiley & Sons, N. Y., 1982, 1997, 2004.

[16] Y.Y. Hu, "Back-Scattering Cross Section of a Center-Loaded Cylindrical Antenna," IRE Trans. A & P, pp. 140-148, Jan. 1958.

[17] D.L. Jaggard, "On Bounding the Equivalent Radius," IEEE Trans. Antennas Propagat., Vol. 28, No. 3, pp. 384-388, May 1980.

[18] E. Hallén, *Electromagnetic Theory*, Chapman and Hall, London 1962.

[19] A. Rubinstein, F. Rachidi, M. Rubinstein, "On Wire-Grid Representation of Solid Metallic Surfaces," IEEE Trans. on Electromagn. Compatibility, Vol. 47, No. 1, pp. 192-195, Feb. 2005.

[20] K.T. McDonald, "Scattering of a Plane Wave by a Small Conducting Sphere," Joseph Henry Laboratories, Princeton University, Princeton, NJ 08544, April 28, 2014.

AUTHOR

Tony Golden – I am an independent researcher with more than 20 years of experience in numerical methods applied to Electromagnetics. My passion for radiating systems has led me to found a software company dedicated to developing tools for antenna simulation. You can reach me at ansof@antennasimulator.com.